MICROMACHINED STIMULATING ELECTRODES

Quarterly Report #6

(Contract NIH-NINDS-N01-NS-5-2335)

January 1997 --- March 1997

Submitted to the

Neural Prosthesis Program
National Institute of Neurological Disorders and Stroke
National Institutes of Health

by the

Center for Integrated Sensors and Circuits
Department of Electrical Engineering and Computer Science
University of Michigan
Ann Arbor, Michigan
48109-2122

April 1997

MICROMACHINED STIMULATING ELECTRODES

Summary

During the past quarter, work has gone forward in a number of areas. Electrochemical characterization of sites exhibiting a large negative open-circuit potential (OCP) appear quite similar to normal sites except for a strong resistive component below 1Hz. Characterization of test electrodes using Ir/Ti and Ti surfaces do not appear to support the generation of these OCPs due to exposed Ti since the OCP for Ti is not sufficiently negative nor is the exchange current sufficiently large. Work to identify the cause of these potentials is continuing. Work to evaluate TiN as an alternative to IrO as a stimulating material does not, as of this writing, support the large charge delivery numbers reported by others recently and indicates that it is not preferable to IrO as a site material. Investigations here are also continuing.

During the last quarter, we have also continued to explore the use of parylene as a conformal insulating layer on the probes. Laser ablation was evaluated as a means for removing the parylene over the site areas and was used successfully in this way. A thin layer of parylene is left on the site following ablation which is then removed using an oxygen plasma. This approach has worked well, producing impedance-frequency plots and CV plots similar to that of normal sites.

Finally, in the area of active probes, we have added the option on our new 2D STIM-2B probe of using it in multi-probe 3D arrays. By adding a simple four-bit register per probe, we allow a given external channel to be routed to any probe in a multi-probe array. This effectively allows another dimension of control over stimulus insertion. During the coming term, we hope to complete the fabrication of the new STIM-2B probes as well as completing the electrochemical characterization of the new site structures and the various materials used for site realization. We will then return to the development of the high-end STIM-2 probes for use in 2D and 3D arrays.

MICROMACHINED STIMULATING ELECTRODES

1. Introduction

The goal of this research is the development of active multichannel arrays of stimulating electrodes suitable for studies of neural information processing at the cellular level and for a variety of closed-loop neural prostheses. The probes should be able to enter neural tissue with minimal disturbance to the neural networks there and deliver highly-controlled (spatially and temporally) charge waveforms to the tissue on a chronic basis. The probes consist of several thin-film conductors supported on a micromachined silicon substrate and insulated from it and from the surrounding electrolyte by silicon dioxide and silicon nitride dielectric films. The stimulating sites are activated iridium, defined photolithographically using a lift-off process. Passive probes having a variety of site sizes and shank configurations have been fabricated successfully and distributed to a number of research organizations nationally for evaluation in many different research preparations. For chronic use, the biggest problem associated with these passive probes concerns their leads, which must interface the probe to the outside world. Even using silicon-substrate ribbon cables, the number of allowable interconnects is necessarily limited, and yet a great many stimulating sites are ultimately desirable in order to achieve high spatial localization of the stimulus currents.

The integration of signal processing electronics on the rear of the probe substrate (creating an "active" probe) allows the use of serial digital input data which can be demultiplexed on the probe to provide access to a large number of stimulating sites. Our goal in this area has been to develop a family of active probes capable of chronic implantation in tissue. For such probes, the digital input data must be translated on the probe into per-channel current amplitudes which are then applied to the tissue through the sites. Such probes generally require five external leads, virtually independent of the number of sites used. As discussed in our previous reports, we are now developing a series of active probes containing CMOS signal processing electronics. Two of these probes are slightly redesigned versions of an earlier first-generation set of designs and are designated as STIM-1A and STIM-1B. A third probe, STIM-2, is a second-generation version of our high-end first-generation design, STIM-1. All three probes provide 8-bit resolution in digitally setting the per-channel current amplitudes. STIM-1A and -1B offer a biphasic range using ±5V supplies from 0μA to ±254μA with a resolution of 2μA, while STIM-2 has a range from 0 to ±127μA with a resolution of 1μA. STIM-2 offers the ability to select 8 of 64 electrode sites and to drive these sites independently and in parallel, while STIM-1A allows only 2 of 16 sites to be active at a time (bipolar operation). STIM-1B is a monopolar probe, which allows the user to guide an externally-provided current to any one of 16 sites as selected by the digital input address. The high-end STIM-2 contains provisions for numerous safety checks and for features such as remote impedance testing in addition to its normal operating modes. It also offers the option of being able to record from any one of the selected sites in addition to stimulation. It will be the backbone of a multi-probe three-dimensional 1024-site array now in development. A new probe, STIM-2B, is currently being added to this set. It offers 64-site capability with off-chip generation of the stimulus currents on four separate channels.

During the past quarter, we have continued to fabricate passive probe structures for internal and external users. A new Kapton-based cable structure is being evaluated for use between short silicon ribbon cables and the percutaneous plug in chronic implant

assemblies. Investigations are continuing into sites exhibiting negative open-circuit potentials and into the use of TiN as a stimulating site material. Laser ablation has been used successfully with parylene coating as an outer insulating layer over probe arrays with an oxygen plasma used to strip the final parylene layer from the sites. Finally, the design of STIM-2B has been extended to achieve compatibility with 3D arrays. The results in each of these areas are described more fully in the sections below.

2. Passive Probe Developments

Work on a "general purpose" passive probe mask set continues. These designs will be used by the Center for Neural Communication Technology to supply external investigators. Probes on this mask are being designed based on input from a survey e-mailed to CNCT probe users. Both single- and multi-shank probes will be included, with shank lengths ranging from 2mm to 2cm and sites spaced from 25μm to 200μm.

As proposed in the last report, we are exploring a potential packaging scheme which will utilize a Kapton-based flex circuit, in conjunction with a short length of silicon cable, as a major portion of the interconnect. These cables are constructed of multiple copper traces sandwiched between 1/2 mil-thick polyimide layers. Acrylic adhesive layers form the bond between the polyimide and copper. Copper traces on these flex circuits can be as narrow as 75μm with a minimum pitch of 150μm.

Cables were designed during the last quarter and were fabricated by a commercial vendor. An unbonded cable intended for use with a 12-pin Microtech receptacle is shown in Fig. 1. The width of this 12-lead cable is 1.9mm and its length is 1.5cm. Traces are exposed several millimeters back from the end to permit ultrasonic bonding to the probe. Solder rings on the flip side of the cable are used for connection to the Microtech.

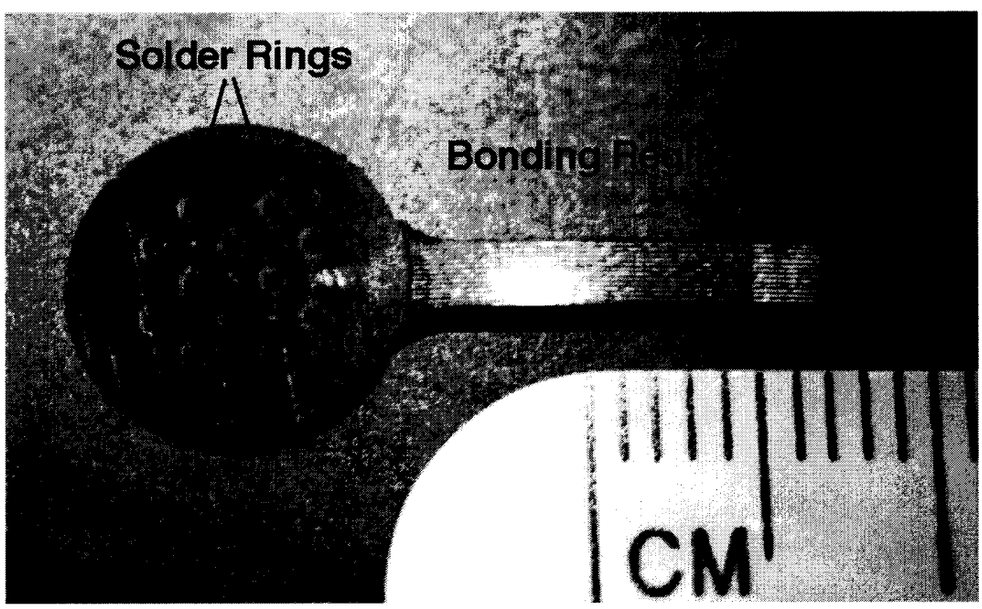

Fig. 1: Kapton flex circuit being explored as possible interconnect component. The structure is composed of multiple copper traces sandwiched between polyimide and acrylic adhesive layers. The design is intended to be soldered to a 12-pin Microtech connector.

As described in the last report, this technique is being investigated in order to improve probe yield and the robustness of chronic assemblies. By decreasing the required length of the silicon cable, we should be able to greatly increase probe yield on a given wafer. The silicon cable will be most likely be <1cm, or the length required to achieve the necessary bends to get the probe into the brain and to take the signals from the probe to the subdural space. The polyimide cable is mechanically robust and will therefore be useful to take the signals from the subdural space through the skull defect and to the percutaneous connector. These polyimide cables can also be made in long lengths, which is a useful feature for some applications such as peripheral nerve and spinal cord. A mock-up assembly, not bonded or potted, is shown in Fig. 2.

Fig. 2: Proposed chronic assembly. A probe with a shortened silicon cable (<1cm) is ultrasonically bonded to the polyimide cable and all exposed connections are then potted.

While this approach appears attractive for the above reasons, there are several challenges which must be met before these assemblies are useful for even short-term chronic experiments. The most critical challenge to be faced is encapsulation. There are several points on the assembly which have a potential for failure. The probe will be attached to the cable and then ultrasonically bonded to the gold-plated traces. This area is probably the most vulnerable to leakage and will be the most difficult to encapsulate since there are a number of different surfaces which must be coated (i.e., the probe, the exposed gold traces on the polyimide cable, polyimide, gold bond wire). The insulating properties of the polyimide itself are also suspect. We are working in conjunction with the MIT group to determine whether the devices can be sufficiently encapsulated. That group has fabricated polyimide test devices of the same basic structure as our cables which are being soak tested using various potting materials under high temperature. In parallel, we are

performing soak tests in our own laboratory. We hope to report results on these initial tests in the next quarter.

3. *Electrochemical Site Characterization*

It has been found that a number of electrodes with the new site design (in which the metal comes up over the field oxide and overlaps adjacent conductors) have open circuit potentials that differ from the value expected for iridium oxide. This anomaly has been investigated and the current findings are presented below.

The open circuit potential (OCP) for iridium (in PBS, vs. SCE) is typically 150mV. On a number of probes, sites have shown an OCP of -250mV. These probes feature sites realized in the new design, with the Ti/Ir site laying on top of the dielectric with contact to the polysilicon conducting line via small interconnect holes. A comparison was made between the impedance spectrum and cyclic voltammagram of two sites, both with the new site design. One site had an OCP = 150mV and the other showed an OCP = -250mV. The impedance magnitudes and phase spectra are plotted below. The impedance was measured at a DC potential of 0.3V (in PBS vs. SCE). The electrodes were not activated. The impedance plots for the two sites are similar, except at low frequency. The site with the positive OCP behaves as expected for iridium at all frequencies. The low frequency response of this site is capacitive, with a phase near 90° and a magnitude inversely related to frequency. The site with the negative OCP behaves capacitively above 1Hz also. However, below the 1Hz, this site exhibits a resistive behavior. That is, the impedance magnitude of this site is not increasing with decreasing frequency and the phase is going to zero. Figures 3 and 4 show these impedance plots for the two sites.

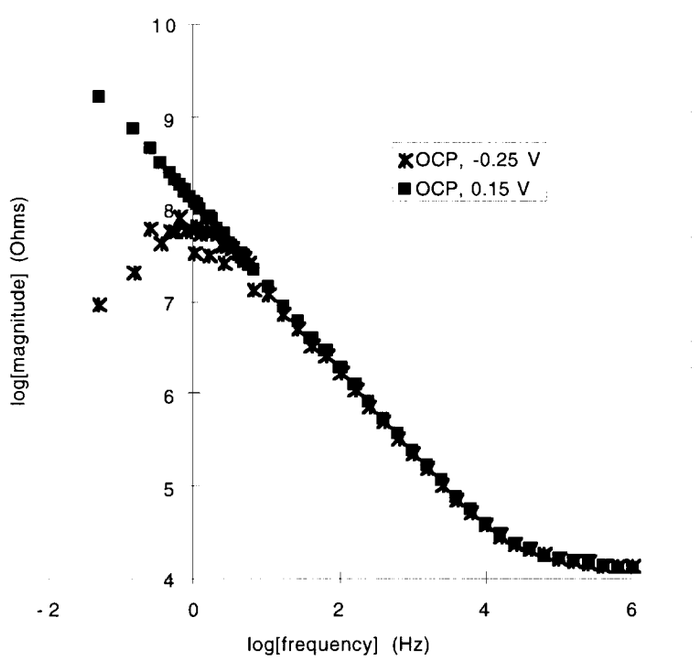

Fig. 3: Impedance Magnitude Spectra of Two Ir Sites with different OCP's

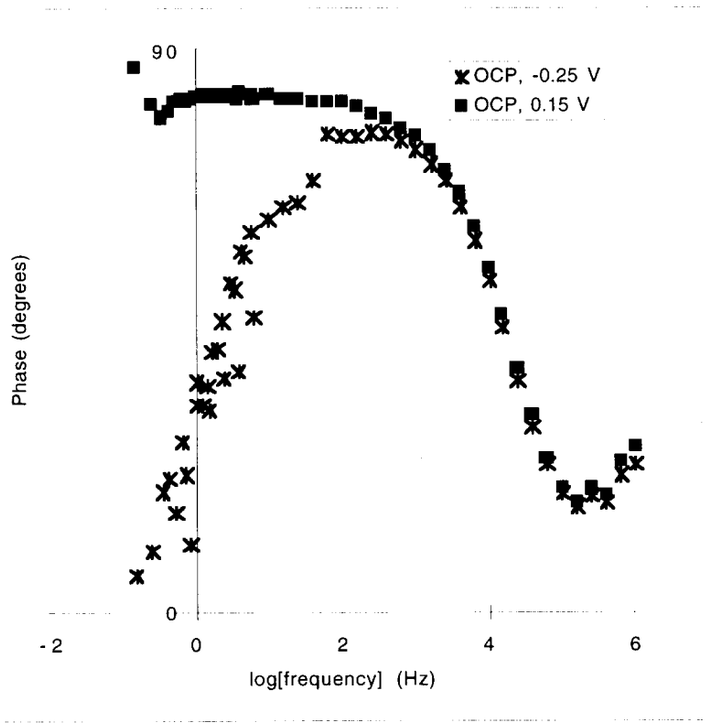

Fig. 4: Impedance Phase Spectra of Two Sites with different OCP's.

The cyclic voltammagrams of the two sites show further deviation from the normal plots for IrO. The CVs were acquired at 100mV/sec in PBS with a SCE reference. The site with the positive OCP shows a capacitive response to the voltage ramp at positive potentials. Again, this is a result consistent with the expected behavior of iridium. The site with the negative OCP has a CV that indicates resistive current flow (current increases with the applied voltage). Figure 5 shows these CVs.

The electrochemical data indicates that the negative open circuit potential is caused by an alternate current path from the electrolyte to a conductor other than iridium. In the example presented above, and in other sites tested, this path appears to have a high impedance and is definitely resistive, which means current is flowing through Faradaic reactions at some other metal. A circuit model of a site that would behave as such is shown in Fig. 6.

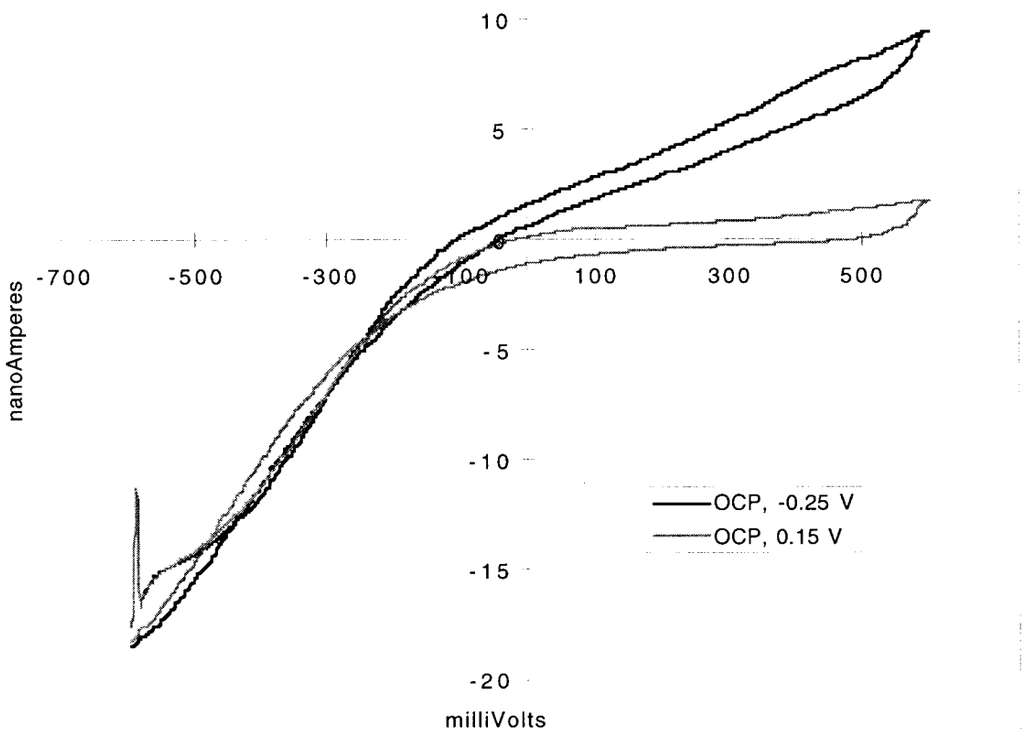

Fig. 5: Cyclic Voltammagrams of Two Sites with different OCP's

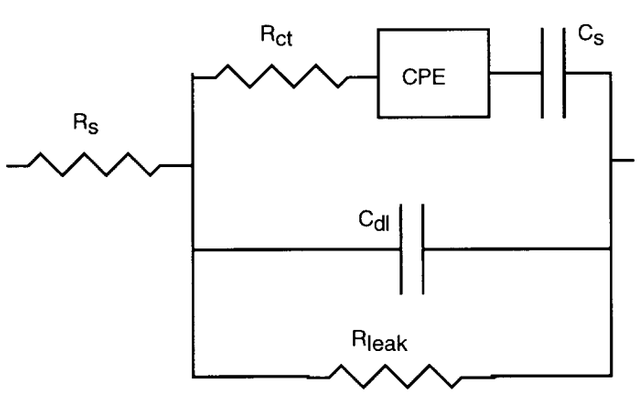

Fig. 6: Circuit model for a site with a negative OCP.

To investigate the source of the negative OCP, titanium and Ti/Ir thin-films were sputtered on silicon wafers. Additionally, samples of titanium nitride (TiN) were prepared. A recent paper suggests that TiN has superior charge injection capability compared to iridium. More on this later. The sputtering procedure for the samples was as follows. The samples were prepared on p-type, 25 ohm-cm, <100>, 4" Si wafers. Each wafer was

dipped in BHF for 20 seconds and immediately loaded into the sputtering machine. In each case, the system pumped down for 1.5 hours which will achieve a base pressure of 50μTorr. The sputtering system will hold 3 targets and therefore will allow dual metal sputtering to occur without the need to break vacuum.

The following table summarizes the parameters used to prepare each of the three metal samples:

Metal	Thickness	Power	RF/DC	Pressure	Ar Flow
Ti	500 Å	700 W	RF	7 mT	30 SCCM
Ti/Ir	500/3000 Å	700W/1A	RF/DC	7 mT	30 SCCM
TiN	1000 Å	700 W	RF	7 mT	30 SCCM

The wafers were diced into smaller sections for testing. A plastic collar was used to define a common surface area for all the samples and the rest of the sample was insulated with a coating of silastic. The OCP of the Ti film was found to be near -50mV, while the Ti/Ir samples generally were around 150-200mV. Current vs. DC potential plots for samples of Ti and Ti/Ir are shown below in Fig. 7.

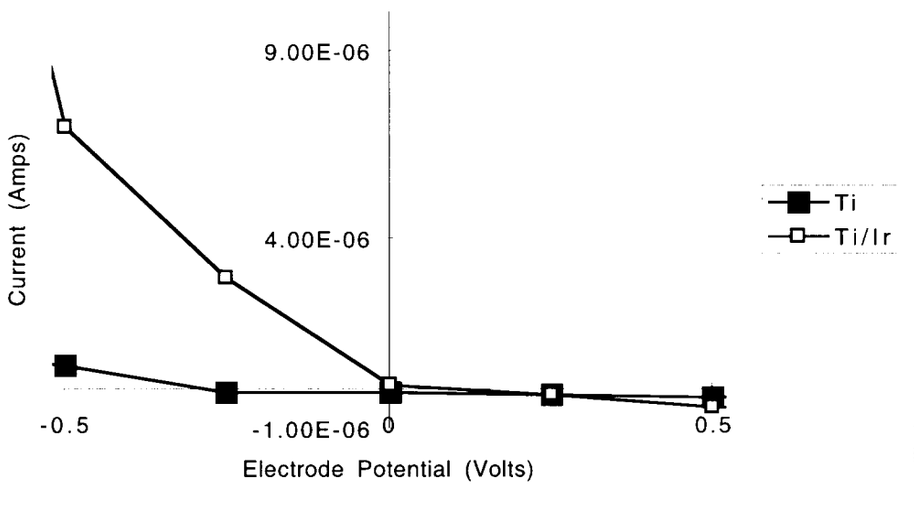

Fig.7: Current vs. DC potential for Ti and Ti/Ir

The OCP measurements of Ti and Ti/Ir thin-films suggest that a simple combination of the two could not result in an OCP of -250mV. The equivalent Ir exchange current density is high, while the value for the Ti is low as expected. If both Ti and Ir were exposed to electrolyte, a reasonable OCP would fall between the individual OCP of the two metals. Experiments run at EIC indicate that the interface electrochemistry between iridium oxide and titanium may lead to a negative OCP. In the next quarter, we will test measure the OCP of polysilicon and perform SEM analysis on sites with negative OCP.

Initial investigations of TiN as a possible stimulating material have produced results contradictory to published data. A recent paper has put the charge storage capacity of TiN at 40 mC/cm^2, comparable to that of activated iridium. Our measurements put Q_{cap} of TiN an order of magnitude below unactivated Ir. It is suspected that some oxide existed on the tested iridium. However, deliberate activation would surely increase Q_{cap} even further. To summarize, our initial results suggest that iridium oxide will have a charge storage capacity at least two orders of magnitude higher than TiN. Futher studies may focus on the sputtering parameters used to create the TiN film in the published result.

4. Use of Parylene Ablation for Site Formation

Recessed electrodes can be formed by coating a probe with parylene and then removing the parylene over the site with a UV laser. A parylene coating can add mechanical strength to the device and aid in biocompatibility. A recessed site will result in a more uniform current density distribution at the electrode-tissue interface. A joint effort with PI Medical (Portland, OR) to investigate methods for applying parylene was begun last fall. Last quarter it was reported that initial testing of the parylene-coated/ablated electrodes indicated that a residual layer of parylene remained on the electrodes. This layer could not be removed by laser without risking damage to the site. It was further reported that gas evolution at the interface (i.e., purposefully violating the water window) removed this residual layer of parylene, effectively cleaning the site. One side effect of electrochemically cleaning the electrodes was that a significant amount of iridium oxide would form during the cleaning process.

A second method of removing residual parylene was explored during the past term. The coating/ablation procedure was described in detail in the last quarterly report and will be reviewed briefly here. Acute electrodes with five sites ($1750\mu m^2$) were coated with parylene and then the parylene above the sites was ablated with a UV laser. A small amount of the parylene was deliberately left on the sites. The probes were processed further with an oxygen plasma etch to remove this residual parylene. This etch will remove parylene uniformly from the probe (i.e., the unablated surface will be etched as well), but the ablation decreases the coating thickness over the site, so etching should open the site well before the unablated coating is removed. The oxygen plasma etch process parameters were 200mTorr, 100mW, and 20SCCM O_2. Exact etch rates are as yet undetermined, but parylene is removed fairly quickly under these conditions. The site was completely opened (as measured by IS) within 5 minutes in most cases (Fig. 8).

Electrode sites were activated and the electrochemical properties were measured using impedance spectroscopy. The sites behaved similarly after oxide formation regardless of the depth of the recess. All sites activated to $30mC/cm^2$ within 200 activation cycles and the cyclic voltammagrams were indistinguishable between recessed and non-recessed sites. The impedance spectra from three recessed electrodes and one non-recessed electrode are plotted below (Fig. 9). As mentioned before, the O_2 etch rate is not yet determined, so the actual depth of the recess is unknown. However, SEM analysis allowed the electrode sites to be placed in order based on relative depth. In Fig. 2, Depth 1 corresponds to the shallowest recess, with Depth 2 and Depth 3 denoting deeper recesses. At the higher frequencies, the impedance is dependent on the recess depth. At this frequency, the impedance is primarily due to the access resistance. The recess limits the access of the electrode to conducting solution and thereby increases the access resistance. The impedance at the lower frequency is due to the diffusion of ions through the porous iridium oxide film. Since all the electrodes have the same Q_{cap}, and, therefore, similar amounts of iridium oxide, the low frequency impedance is independent of the recess.

SEMs of the sites corresponding to the IS data in Fig. 9 are shown (Figs. 10-12). Even though a thin layer of parylene was deliberately left behind, the laser still damaged the sites slightly. Some flaking of the dielectric near the edge of the site is evident.

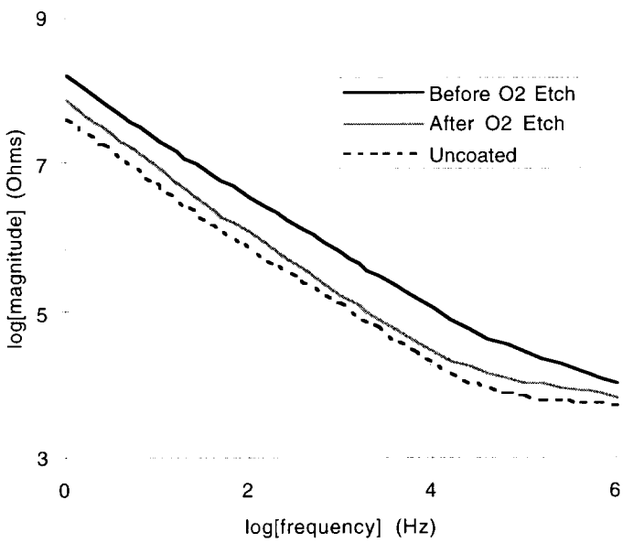

Fig. 8: Impedance Magnitude Spectra of Coated/Ablated Sites Before and After O_2 Etching, Compared with an Uncoated Electrode.

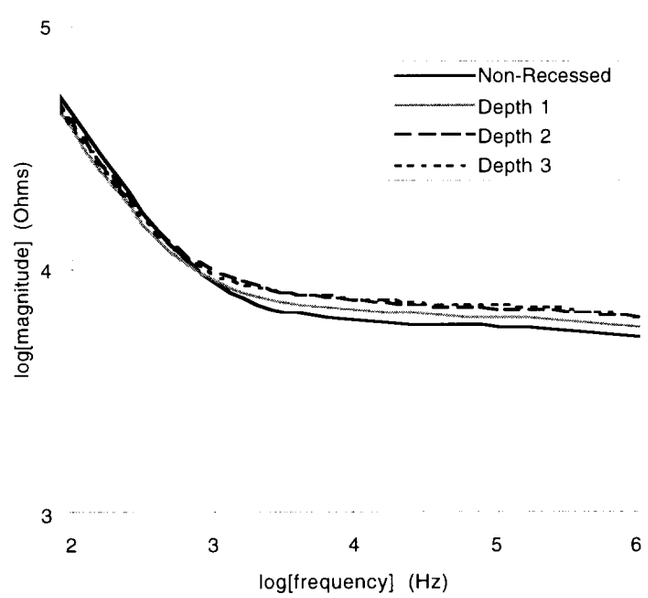

Fig. 9: Impedance Magnitude Spectra for Activated, Recessed Electrodes for Three Recess Depths and an Activated, Non-Recessed Electrode.

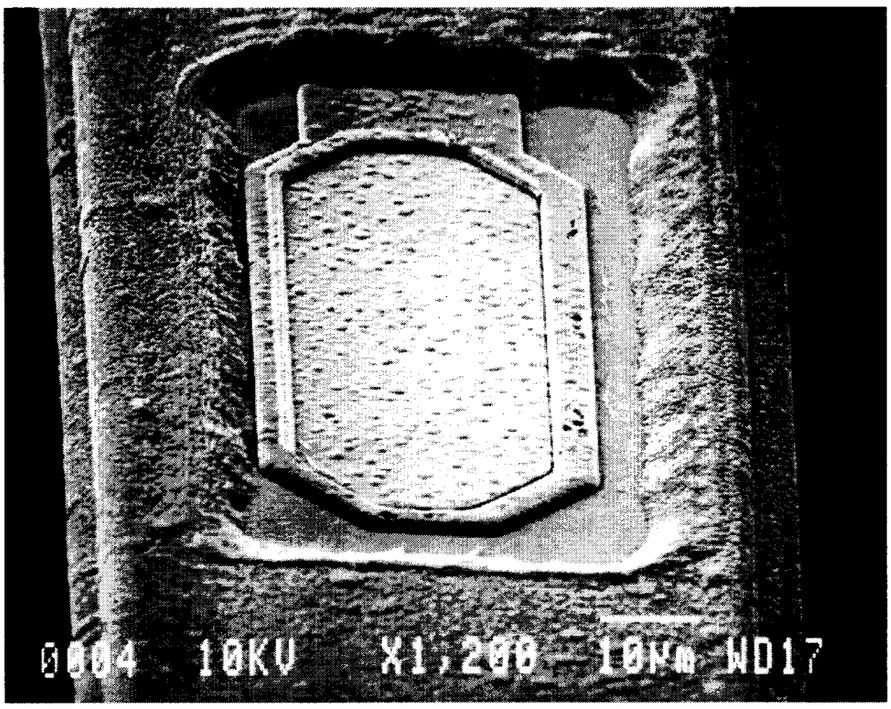

Fig. 10: Depth 1 site, after O_2 etch.

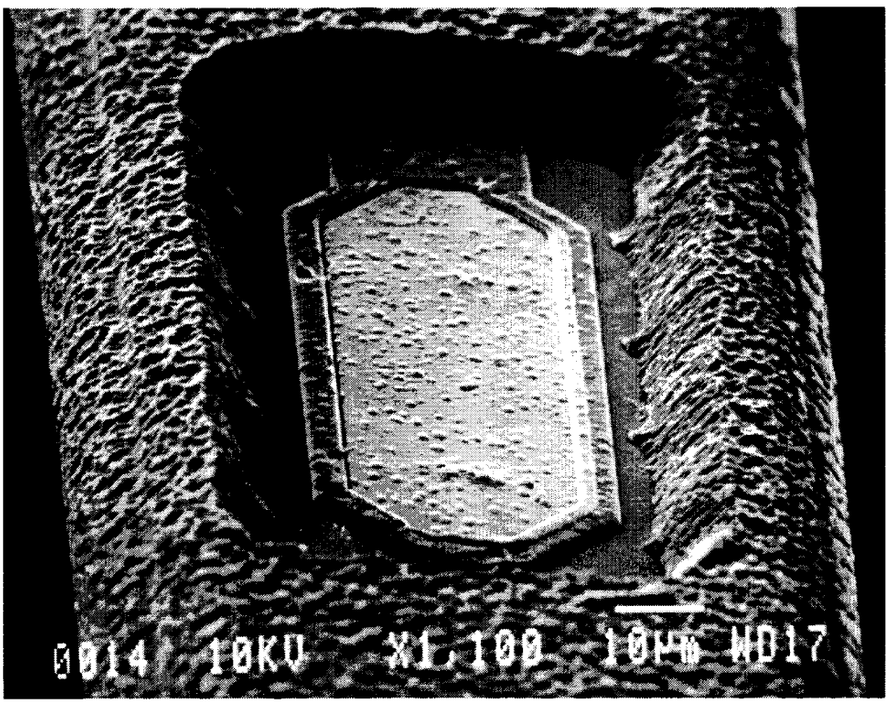

Fig. 11: Depth 2 site, after O_2 etch.

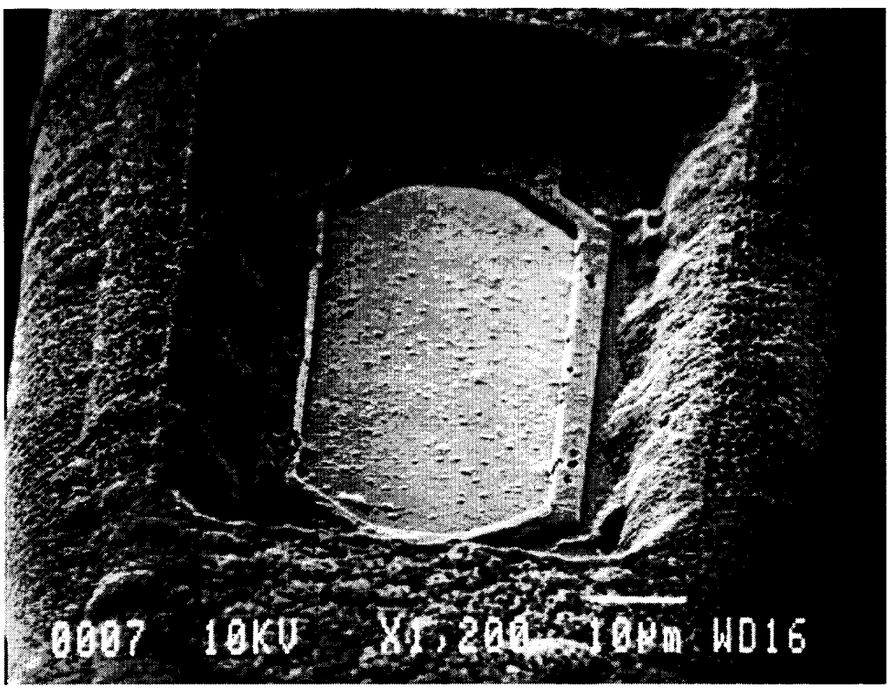

Fig. 12: Depth 3 site, after O_2 etch.

The oxygen plasma proved to be a superior method for opening parylene coated/ablated sites. However, in a few areas around the periphery of the sites, adhesion difficulties were observed between the parylene and the probe. During the next quarter, we hope to quantify the etch rate of parylene in the oxygen plasma and explore the adhesion question in greater depth. Additionally, we will increase the thickness of the protective parylene layer over the electrode to at least a micron to ensure that the laser does not damage the sites.

5. Active Stimulating Probe Development

During the past quarter, the active stimulating probe project has focused primarily on completing the design, simulation and layout of the STIM-2B probe. The possibilities of extending the current STIM-2B design to a 3-dimensional array (STIM-3B) were explored. Several methods of realizing this extension were considered. A virtual register or daisy chain method of interconnecting the probes was chosen to keep the lead count to 10 leads. The necessary alterations of the STIM-2B design and layout were made to realize the STIM-3B probe. Several small issues which arose in the probe designs were also addressed.

STIM-2B

The design, simulation and layout of the second-generation four-channel 64-site version of the simplest active stimulating probe, STIM-1B, which is referred to as STIM-

2B, has been completed. As discussed in the previous progress report, the design utilizes a 20b shift register to load four 4b site addresses which are decoded by a 1-of-16 decoder to connect the designated site to an analog input/output pad through a large CMOS passgate transistor to allow the 'steering' of externally generated currents to the addressed site. The fifth bit is included along with the 4b site address in order to select between the stimulation and a newly added recording function. The fifth bit simply selects either a direct path between the I/O pad and the site or selects the path through an amplifier for simple recording from the same site.

The most important feature of this design is the fact that the probe is almost completely digital. The only analog portions of STIM-2B are the amplifiers. The design is such that if the amplifiers do not function as expected due to bias changes caused by process variations, the probe will still function normally for stimulation. The digital nature of STIM-2B lends itself to a very robust design. This probe is completed and is ready to have the masks made prior to fabrication.

STIM-3B

The STIM-2B design is intended as a simple 2-D active stimulating electrode. With the recent developments in 3-D microassemblies and the use of platform mounting even in the case of 2-D chronic probes, however, we decided to look into the possibility of extending the 2-D design to make it compatible with 3-D arrays. The changes essentially involve structural changes in the probe geometry to accommodate assembly and connection to a platform and any circuit changes necessary to allow addressing of multiple probes. Simply placing multiple copies of STIM-2B on a platform would not work well since we are currently limited to 12 leads by our connector technology. Even only two probes would require 3 shared power lines, 2 clock lines, 1 shared data line, and 8 analog I/O lines. This makes a total of 14 leads, which is over our limit of 12.

Several options were considered for giving STIM-2B a 3D option, and each had its own strengths and weaknesses. The goal is not to expand the number of channels, since the source/sink currents are provided externally on this probe. Rather the goal is to allow these currents to be steered to more sites in a three-dimensional pattern, thus increasing the spatial options for excitation of the tissue. One option considered was to share the I/O lines on a platform bus, which would leave three lines which could be used as enables (i.e., 3 power, 1 clock, 1 data, 4 I/O channels, and three enables). In this case, the design would be straight-forward, but the array would be limited to a three probe 3-D array at most. It should be remembered that the a negative level on either the clock or an enable line can be used to disable stimulation on an entire probe. For this configuration, different addresses could be entered on the different probes but if a stimulus was not desired on a given channel, it could be turned off only by disabling the entire probe. That is, channel A might be directed to site 3 on probe 1 and to site 14 on probe 2; however, if it was not to be used on probe 2, the entire probe would have to be disabled, precluding the use of channels B-D as well. Also, this arrangement could not be used for more than 3 probes without decoding the enables on-chip.

The second and third options considered were simple variations of each other, but would each allow arrays of up to four probes. The first possibility would be to share the four I/O lines and the and clock line (bussing them to all probes in the array), but to have separate address lines and to enable/disable the probes individually by using a negative strobe (the current leak detection state) on the appropriate address line/s, as in Fig. 13.

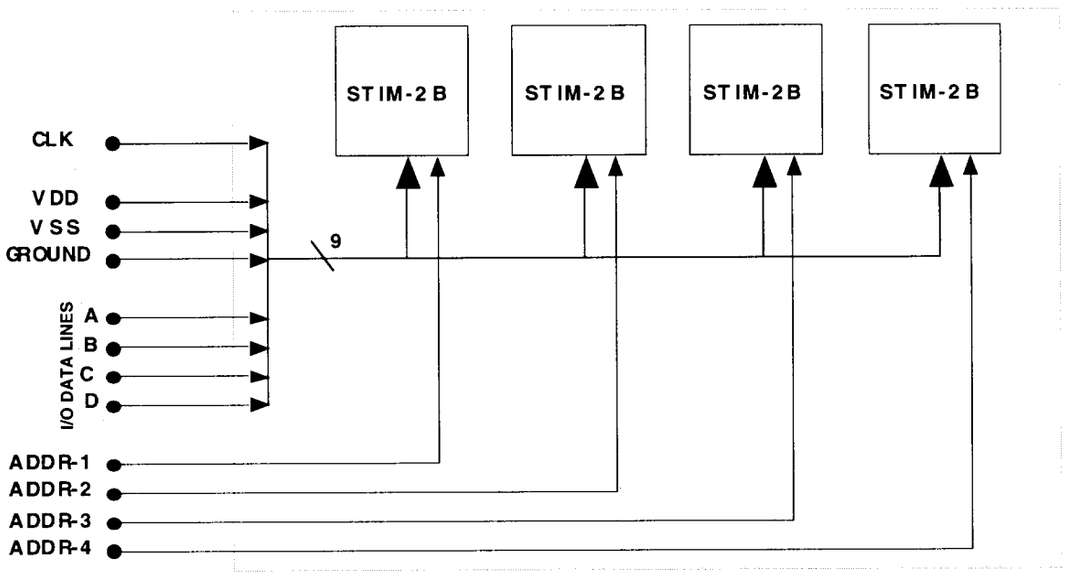

Fig. 13: STIM-3B system utilizing common clock and analog I/O data lines.

The operation would be controlled by a common clock signal which would clock in the site addresses to all of the probes. In this configuration, each probe could receive a different address if desired, although the data would have to be supplied simultaneously. Since the stumulus currents are bussed to all probes, three of the probes would normally be disabled by holding the address line at -5V during the actual stimulus current delivery. The currents could be routed to more than one site but the current splits would depend on the site impedances and would be uncertain.

A small variation of the previous design would be to have a shared address line and individual clock lines for up to four probes in an array as shown in Fig. 14. The operation would be essentially the same as described for the previous option except that the roles of the address and clock lines are switched. The main difference would be seen in interfacing with the external system and in the method in which addresses are changed and probes are selected. These two methods have several pros and cons:

PRO

- simple data structure
- simple circuitry

CON

- not expandable beyond a four probe array
- can only stimulate on one probe at a time, with no inter-probe stimulation, unless uncertain splitting of the stimulus currents is allowed.
- twelve leads

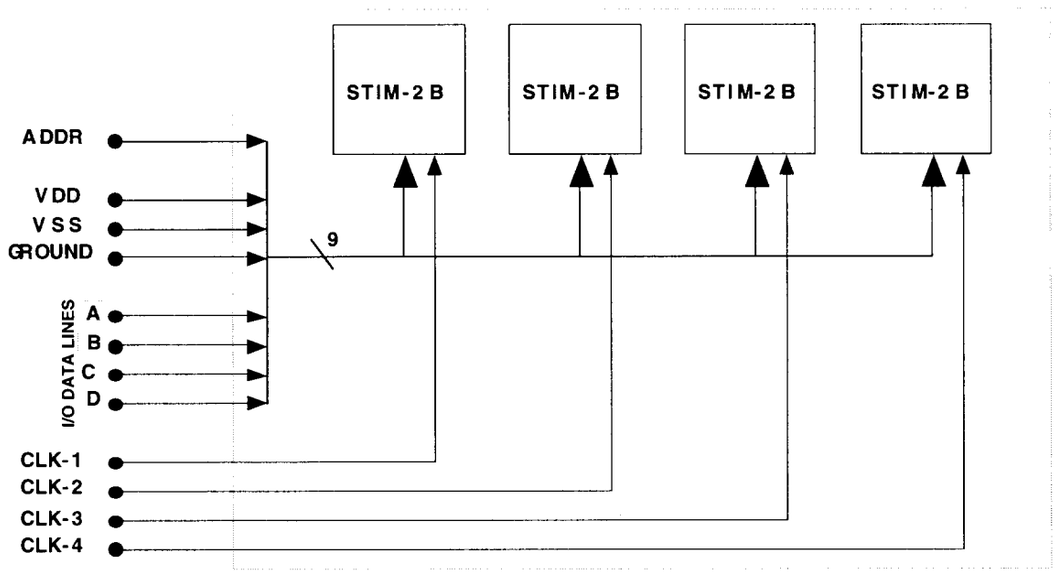

Fig. 14: STIM-3B system utilizing common address and analog I/O data lines.

The final option that was considered is shown in Fig 15. This option requires a modest amount of additional circuitry on each of the probes. An additional 4b shift register is required, with each bit used as a flag bit to enable one of the four I/O lines via a large CMOS passgate. The last bit of the 4b shift register would also be buffered out onto an additional lead to go off probe. The operation of the complete 3-D system is quite simple. All of the probes in the array share common analog I/O data lines, power lines, clock lines and y-addr (normal probe address) lines. The same y-addr is clocked into the 20b shift register on all of the probes.

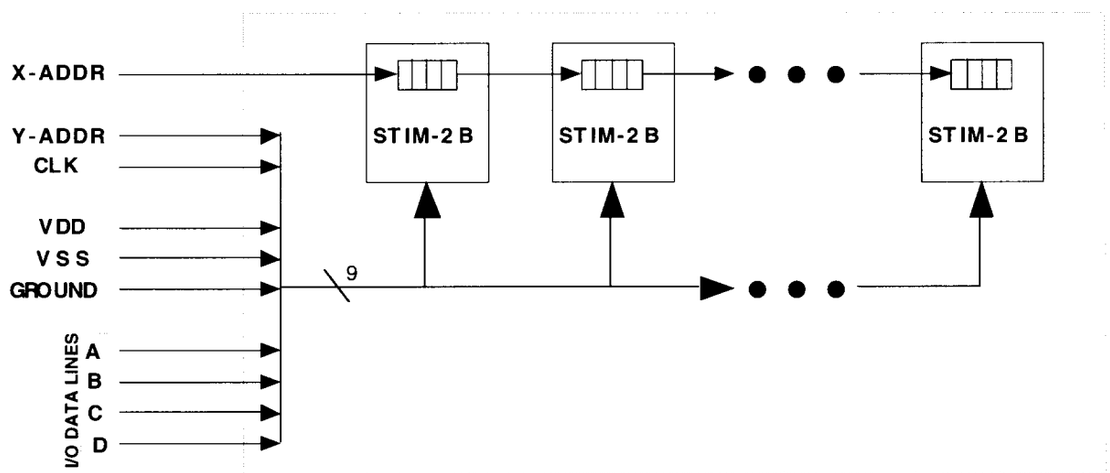

Fig. 15: STIM-3B system utilizing a daisy-chain architecture and a serial per-channel stimulus enable.

The key feature here is that while the y-addr is being clocked into all the probes, an x-addr (I/O channel enable) is simultaneously being clocked into the first probe and daisy-chained to the second, third, and nth probe via interconnecting leads on the platform thus making an extended 'virtual register'. This x-addr allows us to enable or disable each channel on each probe independently from all the others. Differing numbers of probes in the array would result in differing x-addr lengths, but it would only be necessary to be sure that the last bits of both the y-addr and x-addr arrived at the same time. For example, for a 4 probe system, the y-addr would be 20b long as always, but the x-addr would only be 16b long. This means that the actually x-addr data would not begin until the fifth clock time slot as shown in Fig. 16. Alternatively, we could lead with zeros and let them overflow at the end. Theoretically, the size of the array is unlimited because probes can be daisy-chained together indefinitely. Practically, we do not expect to use more than four-probes in any of the initial arrays. The x-address input can be defaulted to the enable state (pulled up on chip) so that no additional external circuitry is needed when used with a single probe. As can be seen, this extendible approach to the 3-D array also has its pros and cons:

PRO

- ten leads
- any combination of four channels across the array
- variable/expandable array size
- inter-probe stimulation capability

CON

- more complex circuitry
- more complex data structure
- y address is common to all probes
- expansion beyond five probes increases data input time

Despite the additional complexities of the system, this last architecture was chosen because of its increased flexibility. The use of a common y-addr for all probes is only awkward if current splitting among sites is allowed. Otherwise, it is not limiting since the x-addr effectively acts as a channel enable on each individual probe. The two additional unused lines also allow space for future functional extensions should they be desirable. Different arrays can also be realized with the same probe by simply changing the platform design. The completed layout of the STIM-3B probe is shown in Fig. 17.

Site Data	F3	D3	D2	D1	D0	F2	C3	C2	C1	C0	F1	B3	B2	B1	B0	F0	A3	A2	A1	A0
Probe/Channel Data	X	X	X	X	J3	J2	J1	J0	I3	I2	I1	I0	H3	H2	H1	H0	G3	G2	G1	G0

Fig. 16: Data structure for the STIM-3B daisy-chained array.

There are some additional fabrication issues that are being addressed in relation to this new set of probes. The first is the problem of protecting the active circuit area from being undercut during the final EDP release etch, while at the same time ensuring that the platform mounting wings of the 3-D probe structure are completely etched clear so that the spacers can properly fit down over them. A blow-up of the wing area of the STIM-3B probe is shown in Fig. 18. This figure shows the method that we will use to ensure that

the area which the spacer must slide down over is etched clear. The angled slots allow a continuous trench to be etched from the front side of the probe even before the etch plane advances from the backside during the final release etch in EDP. The integrity of the circuitry is ensured by making sure the surrounding deep boron diffused rim is wide enough so that the lateral undercut from the corners does not have time to reach the active circuit area.

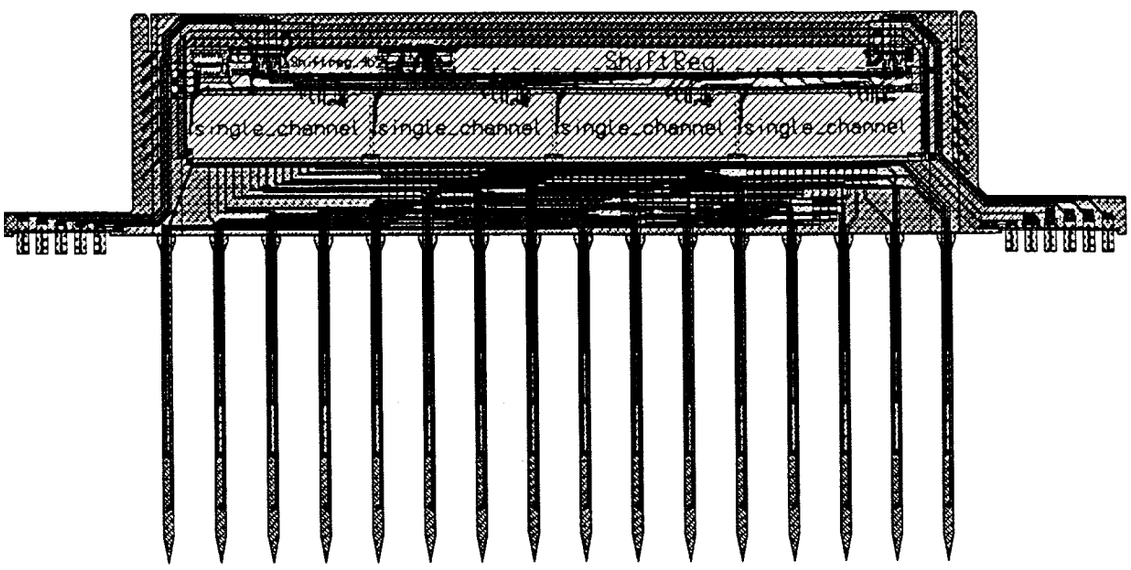

Fig. 17: The final layout of an individual STIM-3B probe.

Another enhancement which has been included on the new STIM-2B and STIM-3B probes is a new three-mask site formation process. In an effort to continue to improve the yield and reliability of the sites, a three-mask site formation process has been developed. Unlike the passive probes, the active probes require a passivation layer of LTO due to the presence of metal interconnect in the active circuitry. This layer of LTO must be at least 1μm thick in order to provide adequate protection in the final EDP release etch. This means that there will be at least a 1μm step covering the polysilicon leads at the site. The large step height can cause significant step coverage problems. The following site formation process will be used which is expected to help reduce step coverage problems and eliminate any possibility of polymer formation problems that have caused problems in the past.

As shown in Fig. 19a, the first mask is used to wet etch the LTO down to the Si_3N_4 and then dry etch (RIE) the Si_3N_4 down to the final layer of LPCVD SiO_2. The second mask, Fig.19b, is then used to open a smaller contact hole through the final SiO_2 layer with a wet etch which does not allow a polymer to form on the polysilicon surface. It also reduces the likelihood of a Si_3N_4 lip forming due to undercutting the SiO_2 layer. The final mask, Fig.19c, is then used to pattern the Ti/Ir site metal via a lift-off process. This

process still allows adjacent leads to pass under the actual site metal thereby reducing the overall shank width.

During the coming quarter, we will work on the fabrication of these active STIM-2B and STIM-3B probes. We anticipate sending out this mask set within a week or so of the writing of this report. The actual platforms and spacers for the 3-D arrays are not included in this mask set, but will be placed in a separate mask set due to their large size and the greatly reduced number of masks required for their fabrication. It would be inefficient to take up a large amount of space on the current mask set, which must be a full CMOS run, when the platforms/ribbon-cables do not require most of these masks.

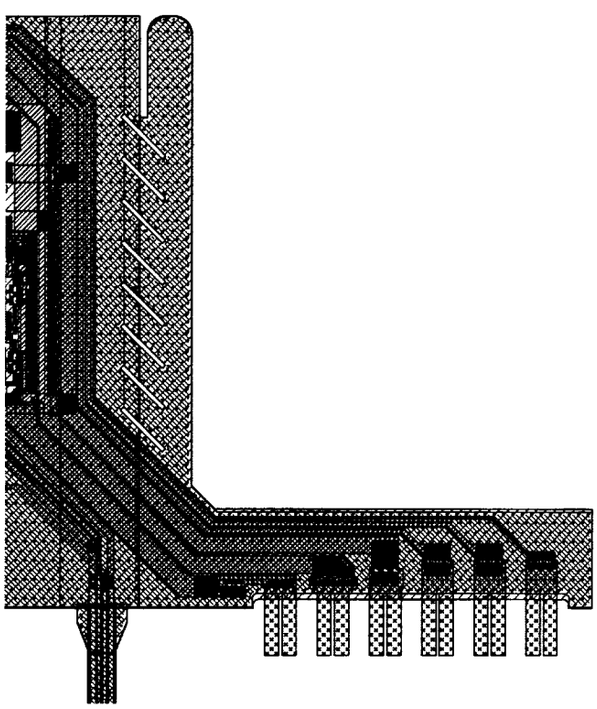

Fig. 18: The wing area of the STIM-3B probe showing the angled slots which ensure the complete undercut of the back-side of the wing area.

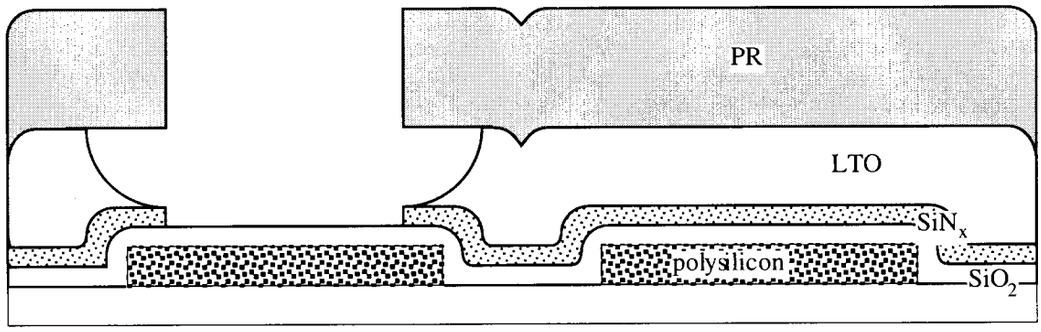

Fig. 19a: Mask #1, wet etch LTO and dry etch Si_iN_4.

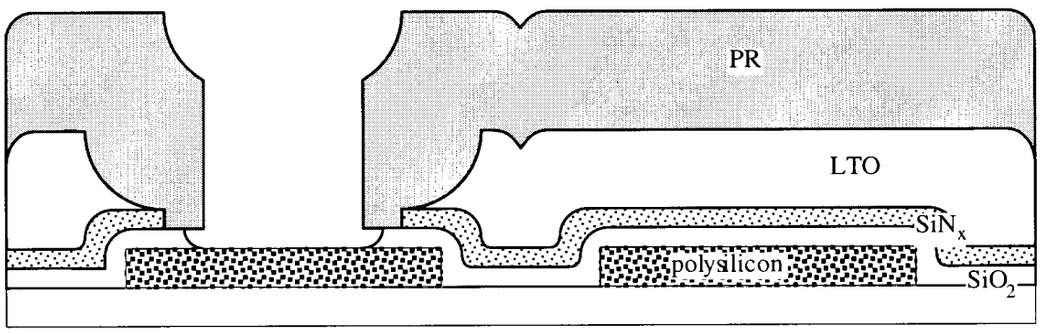

Fig. 19b: Mask #2, wet etch LPCVD SiO_2.

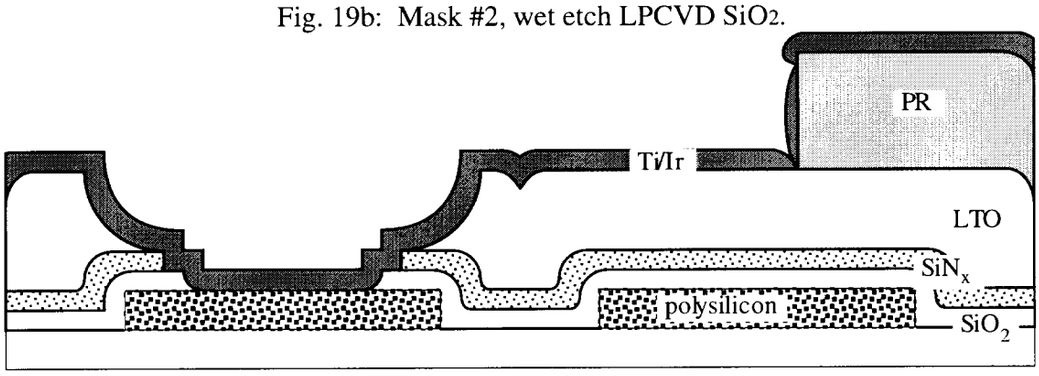

Fig.19c: Mask #3, deposit and lift-off site metal, Ti/Ir.

6. *Development of External Probe Electronics*

During the past quarter, the design for the new external electronic system was updated to support new requirements of the STIM-2B probe design. These requirements include programmable current stimulation circuitry and an extra data line used to implement a serial shift register for selecting an active probe in a multi-probe array. The subsystems designed in support of these new features did not greatly affect the core system design. The core system continues to be a TMS320C26-based DSP system with a serial port UART, fast static memory, and FIFO's for processor-to-probe communication and control line sequencing. The addition of the new components, however, required the redesign of the

address decoding logic to use a programmable element instead of discrete logic for faster operation and a greater number of control lines.

The first new design component consists of an additional data FIFO for storing probe selection information. This FIFO is similar to the probe data FIFO in that it performs parallel-to-serial conversion and, in effect, extends the bit width of the probe data channel from 1 bit to 2 bits. This FIFO will be integrated into the address decoding circuitry so that probe enable data appears to be a part of a normal address selection data word, even though it is actually driving a different data line.

The second new design component is a current generation subsystem. This system consists of a four-unit 8-bit digital-to-analog converter (DAC) with precision ±2.5V reference sources. The DSP processor sees the DAC as a common peripheral device, not much different from other devices such as the UART. Each DAC drives a current source whose circuitry has been modelled on an existing design in use for stimulation experiments. There are four independent and identical current sources corresponding to the four DAC units and the four current lines on the STIM-2B probe. The processor selects a maximum current level by writing an 8-bit word to a given DAC. This 8-bit word is interpreted as a signed binary number, thus allowing both current sourcing and sinking on each current line with 7-bit magnitude resolution. Assuming a maximum current source/sink requirement of 100μA, the 7-bit magnitude resolution will allow current levels to be set with better than 1μA resolution.

Simulation and timing waveforms have been completed for the majority of the new design. These results have cleared the way for the construction of a prototype system on a wire-wrap carrier. Although the basic circuit components are suitable for prototyping, it is unlikely that the entire circuit will be able to operate at maximum speed on a wire-wrap prototype. We therefore expect to use the prototype as a low-speed system for verification of the design and for non-production control of a STIM-2B probe in a test environment. We expect to have the majority of the prototyping effort complete by the next quarter, at least to the point of effecting basic stimulation functions.

7. Conclusions

During the past quarter, work has gone forward in a number of areas. Electrochemical characterization of sites exhibiting a large negative open-circuit potential (OCP) appear quite similar to normal sites except for a strong resistive component below 1Hz. Characterization of test electrodes using Ir/Ti and Ti surfaces do not appear to support the generation of these OCPs due to exposed Ti since the OCP for Ti is not sufficiently negative nor is the exchange current sufficiently large. Work to identify the cause of these potentials is continuing. Work to evaluate TiN as an alternative to IrO as a stimulating material does not, as of this writing, support the large charge delivery numbers reported by others recently and indicates that it is not preferable to IrO as a site material. Investigations here are also continuing.

During the last quarter, we have continued to explore the use of parylene as a conformal insulating layer on the probes. Laser ablation was evaluated as a means for removing the parylene over the site areas and was used successfully in this way. A thin layer of parylene is left on the site following ablation, which is subsequently removed using an oxygen plasma. This approach has worked well, producing impedance-frequency plots and CV plots similar to that of normal sites.

Finally, in the area of active probes, we have added the option on our new 2D STIM-2B probe of using it in multi-probe 3D arrays. By adding a simple four-bit register per probe, we allow a given external channel to be routed to any probe in a multi-probe array. This would effectively allow another dimension of control over stimulus insertion. During the coming term, we hope to complete the fabrication of the new STIM-2B probes as well as completing the electrochemical characterization of the new site structures and the various materials used for site realization. We will then return to the development of the high-end STIM-2 probes for use in 2D and 3D arrays.